Constraint analysis of thickness effects on fracture resistance behavior of clamped single-edge notch tension specimen

Baoming Gong[a], Congcong Xia[a], Giuseppe Lacidogna[b], Quanjun Xu[a], Yong Liu[a,*] and Yizhe Li[c]

[a] *Department of Materials Science and Engineering, Tianjin University, Road Weijin 92, 300072 Tianjin, China*

[b] *Department of Structural Engineering, Geotechnics and Building, Politecnico di Torino, Corso Duca degli Abruzzi 24, 10129 Torino, Italy*

[c] *CRRC Qingdao Sifang Rolling Stock Co. Ltd., Jinhong East Road, 262111 Qingdao, China*

*The correspondence E-mail: lydreamer@tju.edu.cn

Abstract

The correlation between the out-of-plane stress and the in-plane stress is established based on the bending modified *J-Q* theory and the out-of-plane constraint parameter T_Z. Accordingly, an improved *J*-Q_Z-*M* constraint theory is developed to characterize the crack-tip fields by taking into account opening- and bending-dominated deformations in the ligament of the clamped single edge notch tension (SE(T)) specimens. Three-dimensional elastic-plastic finite element analyses (FEA) with a wide range of in-plane and out-of-plane constraints are performed to validate the proposed approach. It is found that the proposed *J*-Q_Z-*M* constraint theory can effectively quantify the crack-tip fields of SE(T) specimens, and the constraint parameter Q_Z exhibits approximately load- and distance-independence under large scale yielding (LSY).

Keywords: *J-Q* theory; SE(T); crack-tip field; constraint;

Nomenclature	
J	J integral
Q	constraint parameter based the J-Q theory
Q_{m}	constraint parameter based the modified J-Q theory
T_{Z}	constraint parameter based the J-T_{Z} theory
Q_{Z}	constraint parameter based the J-Q_{Z}-M theory
σ_0	yield stress
δ_{ij}	Kronecker delta
$\sigma_{ij}^{\mathrm{HRR}}$	HRR solution
$\tilde{\sigma}_{ij}(\theta, n)$	dimensionless stress functions
$\Delta\sigma_M$	additional bending stress
σ^{∞}	the applied stress at the remote ends
L	characteristic length
a/W	crack depth to plate width ratio
B/W	plate thickness to width ratio
v	Poisson's ratio
E	Young's modulus
ρ	radius of the initial blunt notch at the crack tip
C, C'	coefficient relating to the applied load
σ_{xx}, σ_{yy}, σ_{zz}	principal stress
M	global bending moment acting on the ligament
b	ligament length
n	work hardening index
α	hardening constant
I_n	integral constant dependent on n
(r, θ)	the polar coordinates with crack tip as origin
Abbreviations	
SE(B)	three-point bend
C(T)	compact tension
DC(T)	disk-shaped compact tension
SE(T)	single edge notch tension
ASTM	American Society for Testing and Materials
BSI	Bristish Standards Institution
DNV	Det Norske Veritas

1. Introduction

To achieve enough conservatism level and safety margin in structure assessments, standardized fracture toughness testing specimens with deep cracks are designated to guarantee high crack-tip constraint, such as three-point bend SE(B), compact tension C(T) and disk-shaped compact tension DC(T) specimens [1].

However, extensive investigations show that constraint effects have a significant influence on the measurement of fracture toughness [2–6]. The crack and loading configurations recommended in ASTM 1820 [1] may lead to premature maintenances/substitutions in service where structural components generally operate under the low level of crack-tip stress triaxiality, for instance, high pressure piping system and steel catenary riser. Recently, due to the similarity in crack-tip fields and constraint levels between the pressurized full-scale pipe and SE(T) specimens [7–9], surging attention has been paid to analytical and experimental procedures on how to measure fracture toughness using SE(T) specimens. In particular, DNVGL-RP-F108 [10] recommends multiple specimen technique to determine *J-R* curve for both base material and girth welds using SE(T) specimens. CANMET [11] and ExxonMobil [12] developed the SE(T) testing technique, and provided the crack length estimation scheme. BSI 8571 is the first launched standard specified for fracture roughness tests using SE(T) specimen, which comprehensively summarizes the recent progress in the test [13].

Although SE(T) specimen is under low constraint, the specimen geometry still has noticeable effects on ductile fracture, which is characterized by the crack tip constraint level induced by the differences in thickness and remaining ligament [2,4]. Compared to the practical pressurized pipeline under biaxial loading, the out-of-plane constraint loss along the circumferential direction in the standardized SE(T) specimen configuration recommended by DNVGL-RP-F108 [10] and BSI 8571 [13] may lead to significant variation on fracture toughness. Several researchers [2–6,14] have studied the impact of varying constraint effects on fracture toughness by fracture experiments using SE(T), SE(B) and C(T) specimens with different geometrical configurations. Recently, Kalyanam et al. [15] studied constraint effects in slow crack growth test methods for pipe and/elbow test specimens. However, most previous experimental study using SE(T) specimens only considered the influence of a limited number of crack depth variation. The effect of thickness on fracture toughness of SE(T) specimen has not been exhausted yet, which deserves more attention in the view of

structural integrity assessment.

In the study, the effects of out-of-plane constraints (specimen thicknesses) and in-plane constraints (specimen crack lengths) on the fracture toughness of SE(T) specimen are investigated. Based on the three two-parameter theories (the *J*-*Q* theory [16,17], the bending modified *J*-*Q* theory [18] and the *J*-T_Z theory [19,20]), a novel *J*-Q_Z-*M* constraint theory regarding SE(T) specimen is proposed. Through the numerical analyses of the crack-tip constraints, the feasibility of *J*-Q_Z-*M* theory in characterizing the out-of-plane constraints and in-plane constraints of the SE(T) specimens is presented in terms of geometrical independence, load-independence, geometry-dependence and in-plane coupling effects.

2. Overview of crack-tip constraint theories

The quantification of constraints has been investigated extensively in the past few decades. Many constraint parameters as well as fracture theories have been proposed, such as the single-parameter *K* [21] and *J* [22], the two-parameter concepts *K*-*T* [23], *J*-*Q* [16,17], *J*-A_2 [24] for the in-plane constraint and *J*-T_Z for the out-of-plane constraint [19,20]. Although the parameters *T*, *Q*, and A_2 can successfully describe the in-plane constraint, they are incapable of characterizing the out-of-plane constraint at the crack-tip. In the present work, some classic constraint parameters, regardless of in-plane constraint or out-of-plane, are used to calibrate the deviation of crack-tip stress field with increasing thickness.

2.1 *J*-*Q* theory

For elastic-plastic analyses, *J*-*Q* theory was proposed by O'Dowd and Shih [16,17] to characterize the crack tip stress field and quantify the level of constraint. The parameter *Q* (i.e., Q_{HRR}) is defined as a normalized parameter that represents the difference between the crack-tip stress field and HRR solution:

$$\sigma_{ij} = \sigma_{ij}^{HRR} + Q\sigma_0\delta_{ij} \quad \text{at } r > J/\sigma_0 \text{ and } |\theta| < \pi/2 \tag{1}$$

where σ_{ij}^{HRR} is the HRR solution; σ_0 is the yield stress, and δ_{ij} is the Kronecker delta. The HRR solution is

expressed by:

$$\frac{\sigma_{ij}^{HRR}}{\sigma_0} = [\frac{J}{\alpha\varepsilon_0\sigma_0 I_n r}]^{\frac{1}{n+1}}\tilde{\sigma}_{ij}(\theta, n) \quad (2)$$

where J is the J-integral, (r, θ) are the polar coordinates centered at the crack tip, I_n is an integration constant depending on n, and $\tilde{\sigma}_{ij}(\theta, n)$ are dimensionless stress functions. From Eqs. (1) and (2), the parameter Q can be written as:

$$Q = \frac{\sigma_{\theta\theta} - \sigma_{\theta\theta}^{\mathrm{HRR}}}{\sigma_0} \quad \text{at } r = 2J/\sigma_0 \text{ and } \theta = 0 \quad (3)$$

Extensive FEA results indicated that Eq. (1) is approximately valid for most fracture specimens under confined plastic deformation scale. However, the parameter Q is distance-dependent for specimens that are under large applied loads. The J-Q framework was also recently utilized to characterize the out-of-plane constraint of a full plate specimen under bending [25].

2.2 Bending modified J-Q theory

Since J-Q theory cannot characterize the crack-tip stress fields under LSY correctly, Zhu et al. [26] introduced a load-independent constraint parameter Q_{Zhu} to eliminate the effect of bending stress on the crack-tip fields as follows:

$$Q_{\mathrm{Zhu}} = \left[\frac{J}{\alpha\varepsilon_0\sigma_0 I_n L}\right]^{-\frac{1}{n+1}} Q \quad (4)$$

where L is a characteristic length and chosen as 1 mm for convenience. Therefore, the J-Q stress field can be expressed as:

$$\frac{\sigma_{ij}}{\sigma_0} = \left[\frac{J}{\alpha\varepsilon_0\sigma_0 I_n L}\right]^{\frac{1}{n+1}} \times \left[\left(\frac{L}{r}\right)^{\frac{1}{n+1}} \tilde{\sigma}_{ij}(\theta, n) + Q_{\mathrm{Zhu}}\delta_{ij}\right] \quad \text{at } r > J/\sigma_0 \text{ and } |\theta| < \pi/2, \quad (5)$$

According to plasticity theory, the bending stress is approximately proportional to the applied bending moment, and the additional bending stress $\Delta\sigma_M$ could be linearized in the un-cracked ligament:

$$\Delta\sigma_M = -\frac{CM\mathrm{r}}{b^3} \quad (6)$$

where C is the coefficient relating to the applied load. M can be obtained by the applied stress at the remote ends of SE(T) specimens:

$$M = \frac{\sigma^{\infty} aW}{2} \tag{7}$$

Therefore, the J-Q stress field [18] is further modified to:

$$\frac{\sigma_{\theta\theta}(r,0)}{\sigma_0} = \left[\frac{J}{\alpha\varepsilon_0\sigma_0 I_n L}\right]^{\frac{1}{n+1}} \times \left(\frac{L}{r}\right)^{\frac{1}{n+1}} \tilde{\sigma}_{\theta\theta}(0,n) + \left[\frac{J}{\alpha\varepsilon_0\sigma_0 I_n L}\right]^{\frac{1}{n+1}} \times Q_{\mathrm{m}} - \frac{CMr}{\sigma_0 b^3} \tag{8}$$

The coefficient C can be determined by two-point matching method. If the opening stresses determined by numerical analysis at two points $r = r_1$ and $r = r_2$ within the region of interest are denoted as $\sigma_{\theta\theta}^{FEA}(r_1, 0)$ and $\sigma_{\theta\theta}^{FEA}(r_2, 0)$, from Eq. (8), the coefficient C can be written as:

$$C = \frac{\sigma_0 b^3}{M(r_2 - r_1)} \left\{ \begin{array}{c} \left[\frac{J}{\alpha\varepsilon_0\sigma_0 I_n L}\right]^{\frac{1}{n+1}} \times \left(\left(\frac{L}{r_2}\right)^{\frac{1}{n+1}} - \left(\frac{L}{r_1}\right)^{\frac{1}{n+1}}\right) \tilde{\sigma}_{\theta\theta}(0,n) \\ - \left(\frac{\sigma_{\theta\theta}^{FEA}(r_2,0)}{\sigma_0} - \frac{\sigma_{\theta\theta}^{FEA}(r_1,0)}{\sigma_0}\right) \end{array} \right\} \tag{9}$$

With the values of C, the modified constraint parameter Q_{m} can be determined by:

$$Q_{\mathrm{m}} = \left[\frac{J}{\alpha\varepsilon_0\sigma_0 I_n L}\right]^{-\frac{1}{n+1}} \times \left(\frac{\sigma_{\theta\theta}^{FEA}(r,0) - \sigma_{\theta\theta}^{HRR}(r,0)}{\sigma_0} + \frac{CMr}{\sigma_0 b^3}\right) \quad \text{at } r = 2J/\sigma_0 \tag{10}$$

2.3 Out-of-plane constraint parameters

The parameter T_{Z} [19,20] has been used to quantify the out-of-plane constraint effect. The parameter T_{Z} is described as the ratio of the out-of-plane stress (σ_{zz}) to the in-plane stresses (σ_{xx} and σ_{yy}):

$$T_{\mathrm{Z}} = \frac{\sigma_{zz}}{\sigma_{xx} + \sigma_{yy}} \tag{11}$$

Although T_{Z} can explain the thickness effect to some extent, it appears to be unable to characterize the fracture toughness quantitatively. It requires further endeavor to construct a parameter that can interpret the impact of out-of-plane constraint on the fracture toughness both experimentally and numerically.

2.4 Out-of-plane extension of bending modified J-Q theory

It can be seen from the above theories that the ideal constraint parameters for characterizing the three-dimensional crack stress field should satisfy three conditions: (a) distance-independent (b)

load-independent (c) the influence of σ_{zz} being considered. Therefore, it can be inferred that neither the bending modified *J-Q* theory nor the out-of-plane constraint parameter T_Z can accurately describe the out-of-plane constraint effect of the SE(T) specimens. Based on above mentioned theories, this paper proposes a modified solution of the *J-Q* theory to describe the three-dimensional crack of the SE(T) specimens.

According to Eq. (11), when considering a three-dimensional SE(T) specimen subjected to both tensile and bending, the out-of-plane stress (σ_{zz}) is proportional to the sum of the in-plane stresses (σ_{xx} and σ_{yy}):

$$\sigma_{zz}(r,0) = (\sigma_{xx}(r,0) + \sigma_{yy}(r,0)) \times T_Z \tag{12}$$

A parameter Q_Z considering the three-dimensional crack effect can be introduced according to Eq. (8), and the out-of-plane stress (σ_{zz}) is expressed as:

$$\frac{\sigma_{zz}}{\sigma_0} = \frac{\sigma_{zz}^{HRR}}{\sigma_0} + \left[\frac{J}{\alpha\varepsilon_0\sigma_0 I_n L}\right]^{\frac{1}{n+1}} \times Q_Z - \frac{C'Mr}{\sigma_0 b^3} \tag{13}$$

where σ_{zz}^{HRR} is the *z*-direction HRR stress field and *C'* is the linearization factor. Considering Eq.(8) and Eq.(12), σ_{zz}^{HRR} can be defined as:

$$\sigma_{zz}^{HRR} = (\sigma_{xx}^{HRR} + \sigma_{yy}^{HRR}) \times T_Z \tag{14}$$

The parameter Q_Z in Eq. (13) and Eq. (14) considers the influence of out-of-plane stress (σ_{zz}) on the stress field of the crack front. And it is both distance independence and load independence, which will be further discussed in the following section. The calculation of Q_Z and *C'* are similar to the Eq. (9) and (10) in Section 2.2 and can be described as follows:

$$C' = \frac{b^3}{M(r_2 - r_1)} \times \left[\sigma_{zz}^{HRR}(r_2,0) - \sigma_{zz}^{HRR}(r_1,0) - (\sigma_{zz}^{FEA}(r_2,0) - \sigma_{zz}^{FEA}(r_1,0))\right] \tag{15}$$

$$Q_z = \left[\frac{J}{\alpha\varepsilon_0\sigma_0 I_n L}\right]^{-\frac{1}{n+1}} \times \left(\frac{\sigma_{zz}^{FEA} - \sigma_{zz}^{HRR}}{\sigma_0} + \frac{C'Mr}{\sigma_0 b^3}\right) \quad \text{at } r = 2J/\sigma_0 \tag{16}$$

3. Numerical simulation and results

3.1 Specimen geometries and material properties

SE(T) specimens with six different thicknesses (*B/W*) and four different crack depths (*a/W*) were extracted longitudinally from an API X80 pipeline. The specific dimensions of the specimens are listed in Table 1. Side grooves with a root radius of 0.5 mm, a 15% local thickness reduction, and an angle of 45° are introduced [11], as shown in Fig. 1. The tensile properties of X80 were measured at room temperature using round bars specimen with a diameter of 12.5 mm [27]. The true stress-strain curve of X80 pipeline steel is presented in Fig. 2. For elastic-plastic materials, the uniaxial strain-stress behavior can be described by the Ramberg-Osgood power-law relationship:

$$\frac{\varepsilon}{\varepsilon_0} = \frac{\sigma}{\sigma_0} + \alpha(\frac{\sigma}{\sigma_0})^n \tag{17}$$

where σ_0 is the yield stress, $\varepsilon_0 = \sigma_0/E$ is the yield strain, E is the Young's modulus, α is a hardening constant and n is the strain hardening exponent. It can be concluded from the curve that the 0.2% offset yield stress, the ultimate tensile stress, Young's modulus, the hardening constant, and the strain hardening exponent are 554 MPa, 728 MPa, 206 MPa, 4.04 and 10, respectively. Furthermore, for n=10, $I_n \approx 4.7679$, $\tilde{\sigma}_{rr}(0) \approx 1.7245$, and $\tilde{\sigma}_{\theta\theta}(0) \approx 2.4972$ for HRR solution. The Poisson's ratio is 0.3.

Table 1 Geometrical parameters of SE(T) specimens in FEA.

B/W (-)	a_0/W (-)	*B* (mm)	B_N (mm)	*W* (mm)	*H* (mm)
0.5	0.4	9	7.65	18	180
1	0.2,0.3,0.4,0.5	18	15.3	18	180
2	0.4	36	30.6	18	180
3	0.4	54	45.9	18	180
4	0.4	72	61.2	18	180
6	0.4	108	91.8	18	180

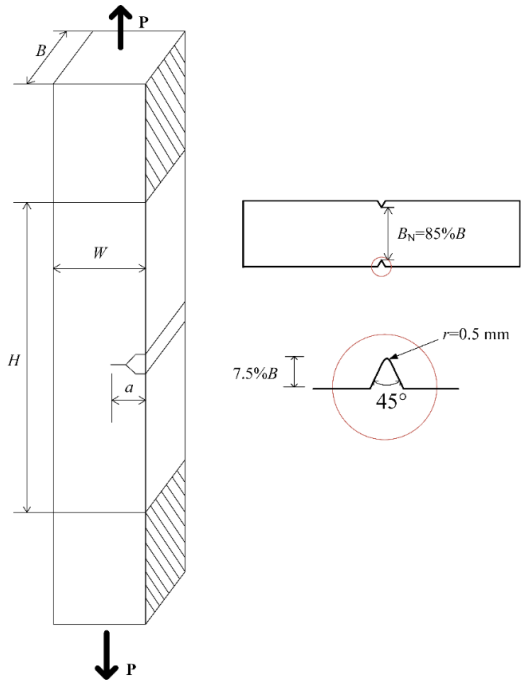

Fig. 1. SE(T) specimens and their geometrical dimensions.

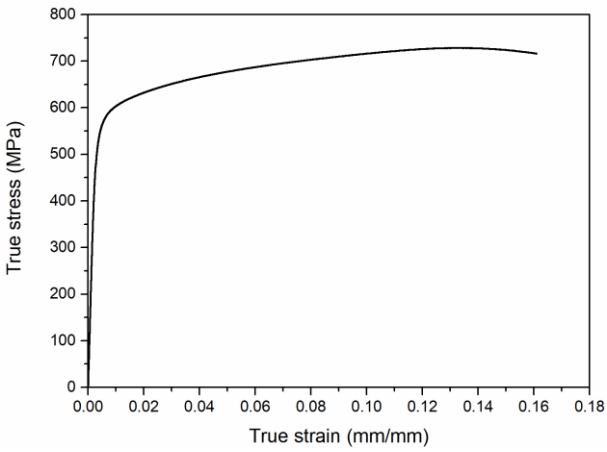

Fig. 2. True stress–strain curve of API X80 steel.

3.2 Finite element modelling

In the study, the full-field 3D elastic-plastic FEA were conducted using ABAQUS 6.14-5. The element type used is 8-node linear brick element (C3D8). A typical FE model (a/W = 0.4 and B/W = 1), as well as the boundary and loading conditions, is shown in Fig. 3. The crack is assumed to be stationary in the analyses; a

root radius (ρ) of 2.5 μm was modeled to facilitate the convergence of the strain analysis (see Fig. 3(b)). A refined spider-web mesh was applied to the blunt crack tip (Fig. 3(b)). Due to symmetry, only one-quarter of the specimens were modeled. To simplify the mesh structure of the finite element model, a sharp V-notch with an opening angle of 45° was used to simulate the passivated side groove of the actual specimen, as shown in Fig. 3(c).

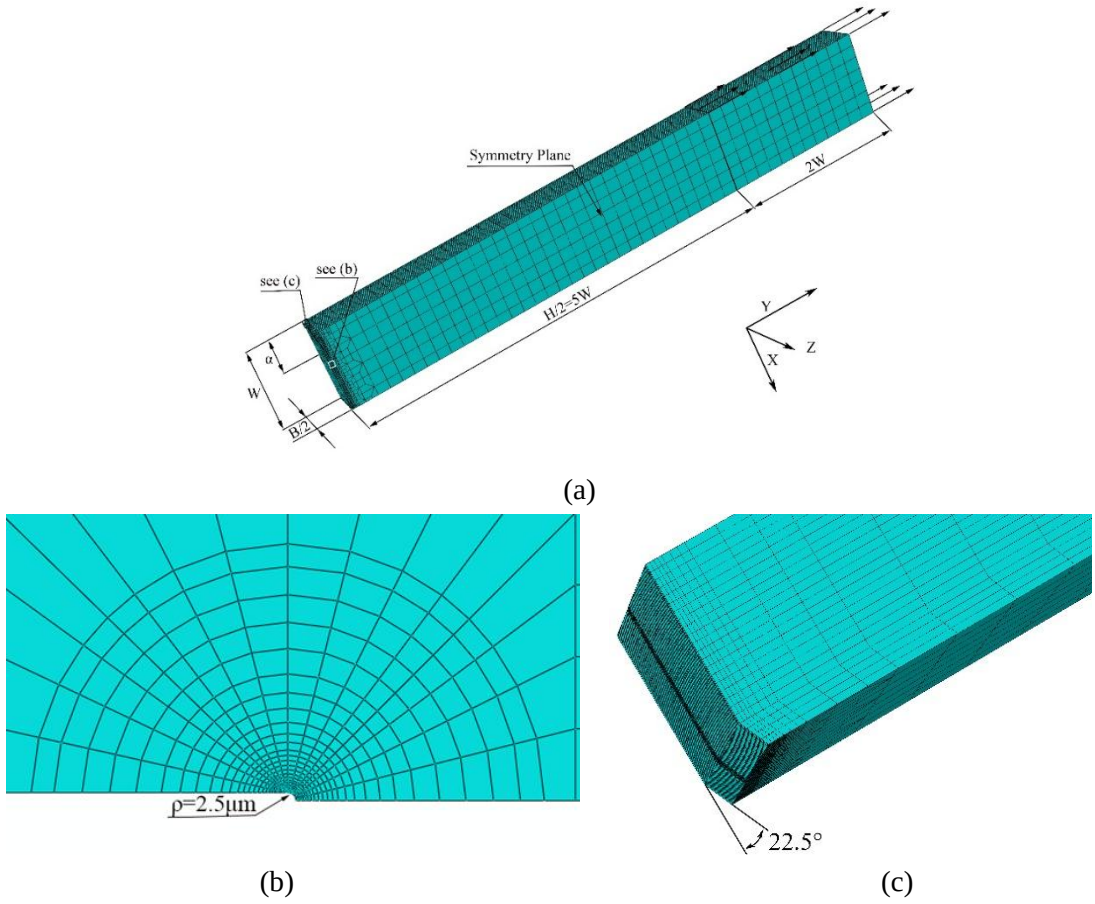

Fig. 3. FE model of SE(T) specimens with a/W = 0.4 and B/W = 1: (a) boundary conditions and meshing configurations; (b) mesh around the blunt crack tip; (c) configuration of the side groove.

3.3 Constraint analyses

3.3.1 In-plane constraint analyses by Q, Q_m and T_Z

In Figs. 4(a)-(d), the distributions of Q (Q_{HRR}) along the ligament are displayed for different crack depths at four different loading levels. Fig. 4 indicates that the values of the constraint parameter Q decrease

gradually as distance r from the crack tip increases under all conditions. Furthermore, it can be found that the decrease in Q under the LSY condition is larger than that under SSY for cracks. The relationship between Q and J for SE(T) specimens at the normalized distance of $r = 2J/\sigma_0$ is presented in Fig. 5. The constraint parameter Q decreases rapidly as loading increases for SE(T) specimen with the same crack length and a strong load sensitivity can be observed. To some extent, this result reflects the effect of the global bending stress on the crack-tip fields of the bending specimen under LSY. Moreover, the in-plane constraint level increases as the crack length increases under SSY. Figs. 4 and 5 indicate that the constraint parameter Q is strongly distance-dependent and load-dependent for all considered situations.

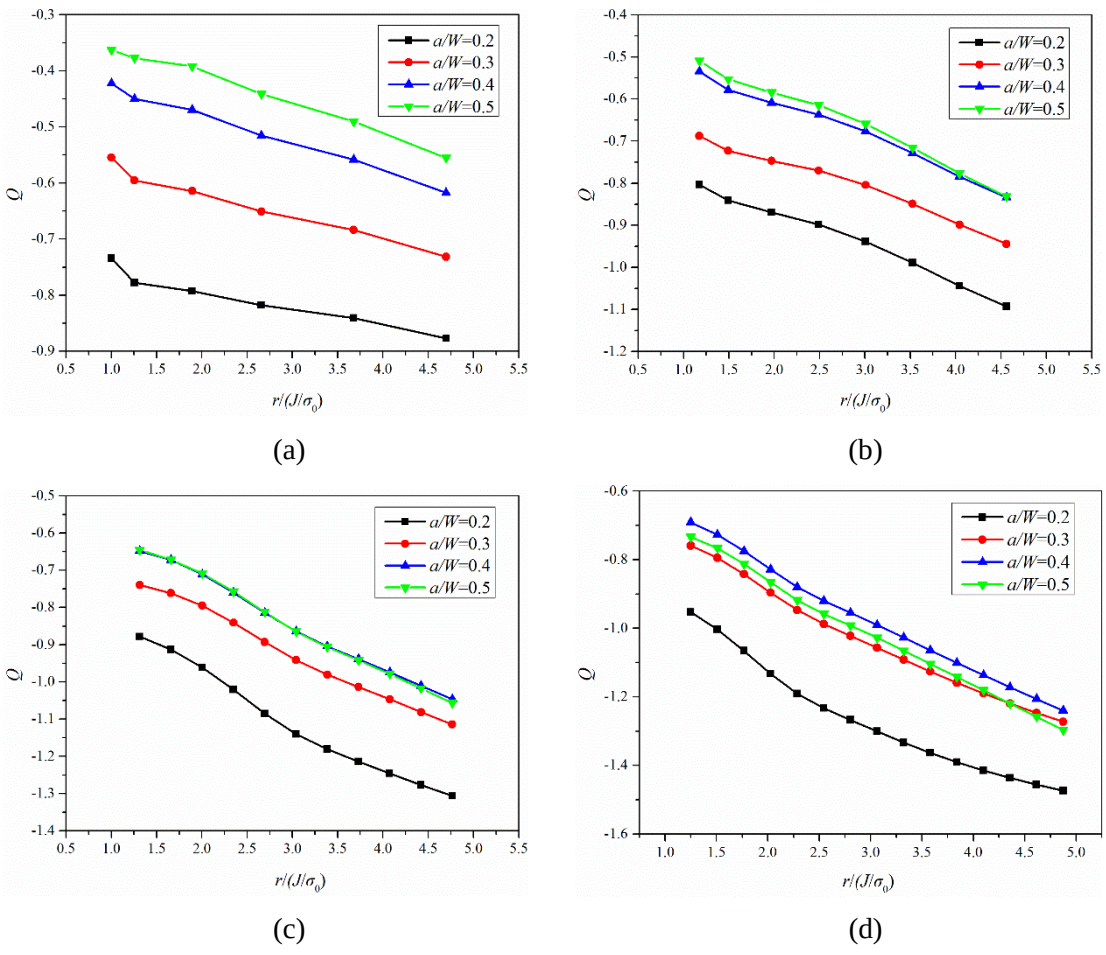

Fig. 4. Distribution of Q along the un-cracked ligament from the crack tip for SE(T) specimens with B/W = 1 and various a/W ratios at applied loading level of (a) J = 50 N/mm, (b) J = 200 N/mm, (c) J = 300 N/mm, and (d) J = 400 N/mm.

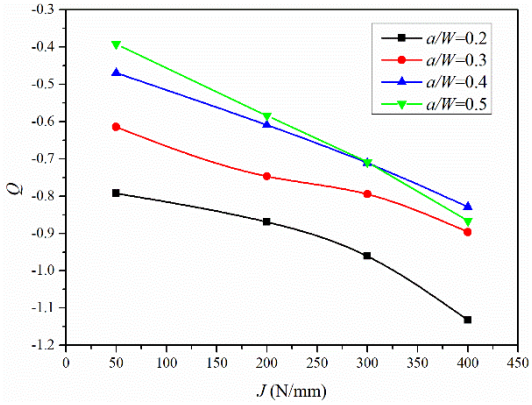

Fig. 5. Variation of Q with J for SE(T) specimens with $B/W = 1$ and various a/W ratios at the normalized distance of $r = 2J/\sigma_0$.

It is shown in Fig. 6 that the constraint parameter Q_m determined by the bending modified J-Q solution (see Eq. (10)) is obtained under the same condition with that of the constraint parameter Q. Fig. 6 indicates that the bending modified parameter Q_m is almost distance-independent within the region of interest under different applied load levels. This result also indicates the significant effect of the global bending stress on the crack-tip fields of the bending specimen. The variations of Q_m with J for SE(T) specimens at the normalized distance of $r = 2J/\sigma_0$ are presented in Fig. 7, where the bending modified constraint parameter Q_m is almost constant as loading increases within the region of interest for SE(T) specimen with the same crack length. The results demonstrate that the constraint parameter Q_m is nearly distance-independent and load-independent.

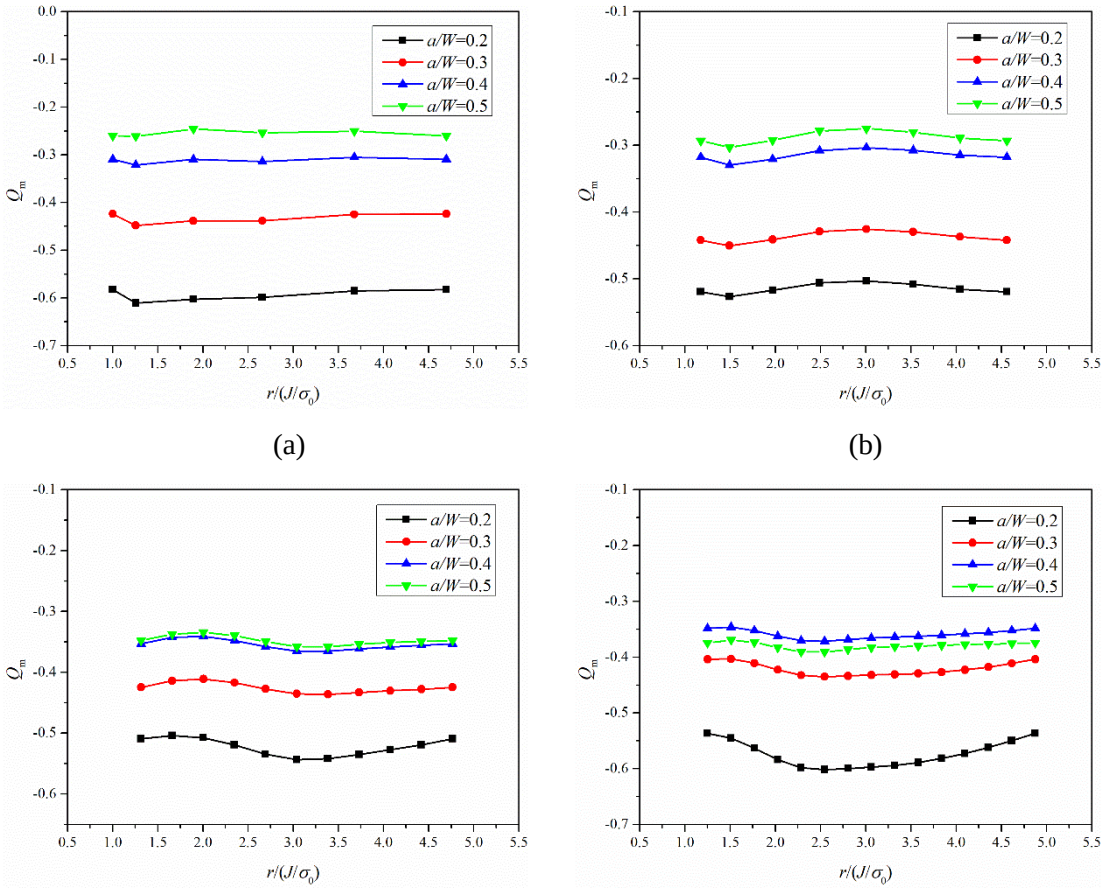

Fig. 6. Distribution of Q_m along the uncracked ligament from the crack tip for SE(T) specimens with B/W = 1 and various a/W ratios at applied loading level of (a) J = 50 N/mm, (b) J = 200 N/mm, (c) J = 300 N/mm, and (d) J = 400 N/mm.

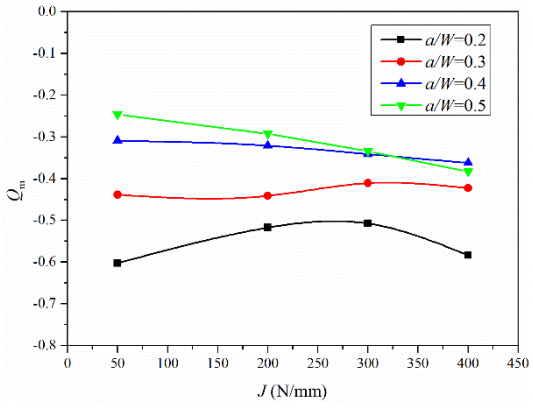

Fig. 7. Variation of Q_m with J for SE(T) specimens with B/W = 1 and various a/W ratios at the normalized distance of $r = 2J/\sigma_0$.

Fig. 8 shows the numerical results of the constraint parameter T_Z determined by Eq. 11 are obtained

under the same condition with that of the constraint parameter Q. It can be seen in Fig. 8 that the parameter T_Z is distance-dependent, with the value decreasing gradually as the distance r from the crack tip increases. Furthermore, the distance-dependence of T_Z increases with the increase of the load levels.

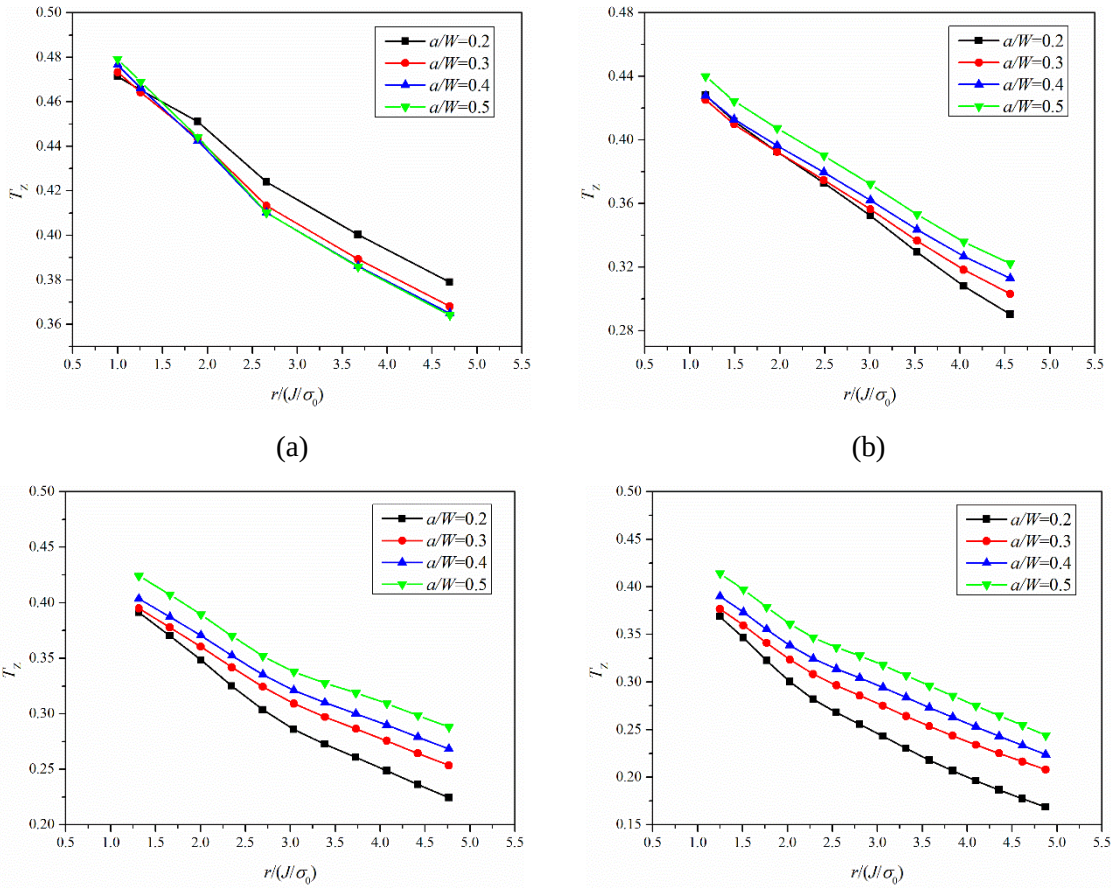

Fig. 8. Distribution of T_Z along the un-cracked ligament from the crack tip for SE(T) specimens with B/W = 1 and various a/W ratios at applied loading level of (a) J = 50 N/mm, (b) J = 200 N/mm, (c) J = 300 N/mm, and (d) J = 400 N/mm.

Fig. 9 illustrates the relationship between T_Z and J for SENT specimens at the normalized distance of $r = 2J/\sigma_0$. It is found that the parameter T_Z decreases rapidly as loading increases for the same crack length, showing very high load sensitivity. Moreover, the out-of-plane constraint level increases slightly with the increase of the crack length for the SE(T) specimens under LSY. Therefore, it can be known that T_Z is not

sensitive to crack length of the SE(T) specimens. It can be concluded from Figs. 8 and 9 that the constraint parameter T_Z is strongly distance-dependent and load-dependent.

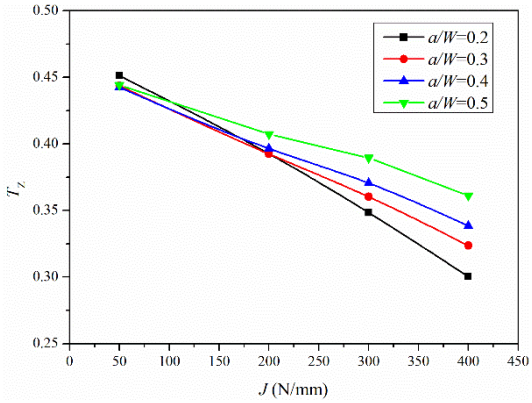

Fig. 9. Variation of T_Z with J for SE(T) specimens with B/W = 1 and various a/W ratios at the normalized distance of $r = 2J/\sigma_0$.

3.3.2 Out-of-plane constraint analyses by Q, Q_m and T_Z

Fig. 10 shows the distribution of Q along the ligament of the SE(T) specimens at four loading levels from SSY to LSY. The results are obtained from FEA results and six different thicknesses are discussed, i.e. B/W = 0.5, 1, 2, 3, 4 and 6, respectively. Fig. 10 shows that for all SE(T) specimens, Q varies along the crack at various load levels, showing strong distance-dependence. Moreover, the distance-dependence of Q increases with the increase of the load levels. The variations of Q with J for SE(T) specimens at the normalized distance of $r = 2J/\sigma_0$ are presented below in Fig. 11. Fig. 11 indicates that the constraint parameter Q reduces rapidly as loading increases for all specimens with the same B/W ratio, representing an active load sensitivity. This result reflects that to some extent the global bending stress has an impact on the crack-tip fields of the bending specimens under LSY. In addition, it is noted that in Fig. 11, Q has a maximum value when B/W=1, and there is no monotonic relationship between Q and the thickness of the specimens. In other words, Q is not sensitive to the thickness of the specimen. As a result, the out-of-plane constraint effect of the

SE(T) specimens cannot be characterized.

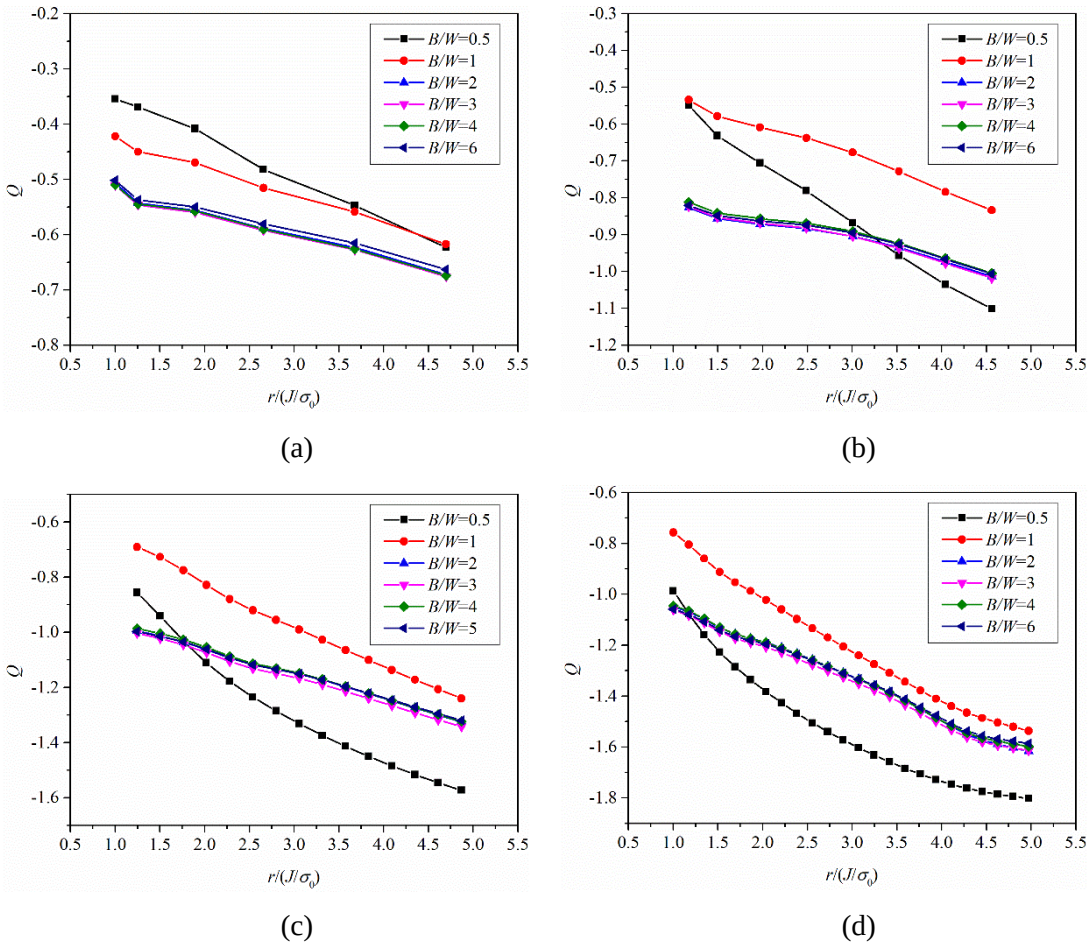

Fig. 10. Distribution of Q along the un-cracked ligament from the crack tip for SE(T) specimens with a/W = 0.4 and various B/W ratios at applied loading level of (a) J=50 N/mm, (b) J=200 N/mm, (c) J=400 N/mm, and (d) J=600 N/mm.

In addition to the situation where the ratio of thickness to width for specimen is 0.5 under LSY, the bending modified parameter Q_m is almost distance-independent within the region of interest in Fig. 12 under SSY and LSY. Further, the parameter Q_m varies greatly for the specimen with B/W = 0.5. This result also indicates the significant effect of the global bending stress on the crack-tip fields of the bending specimens.

Compared with Fig. 11, it is shown in Fig. 13 that the modified parameter Q_m remains constant at the same load level. However, there is an intersection between the curve of B/W = 0.5 and the curve of B/W = 1

at medium load level. In addition, for specimens whose *B/W* is 0.5 and 1, the higher constraint level which is characterized by Q_m is inconsistent with the known facts. Therefore, Q_m cannot characterize the out-of-plane constraint effect of SE(T) specimens. For a reason that Q_m is proposed based on the plane strain condition, the effect of secondary moment on the stress-strain field is not considered [19].

Fig. 14 indicates that the parameter T_Z decreases rapidly with the increase of the distance *r* for specimens with the same *B/W*, i.e. highly distance-dependent. Furthermore, with the increase of the load levels, the difference among T_Z obtained along the crack becomes larger. For SE(T) specimens of $B/W \geq 2$, it can be seen from Fig. 15 that T_Z exhibits excellent load independence. However, for low constraint specimens whose *B/W* = 0.5 and *B/W* = 1, T_Z shows an active load sensitivity. Moreover, the load sensitivity of T_Z increases with the decrease of specimen thickness. It can be seen that T_Z is more sensitive to the out-of-plane constraint effect of SE(T) specimens. However, when the out-of-plane constraint level is high, the differences among T_Z become negligible.

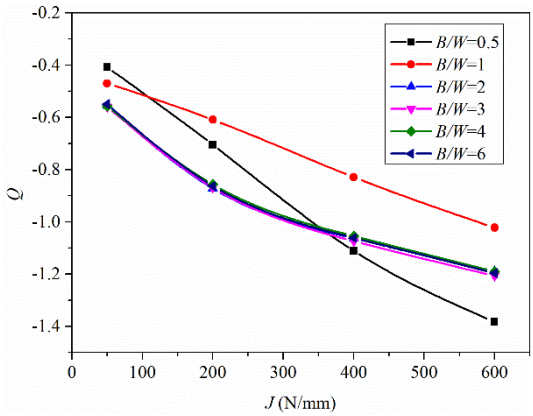

Fig. 11. Variation of *Q* with *J* for SE(T) specimens with *a*/*W*=0.4 and various *B/W* ratios at the normalized distance of $r=2J/\sigma_0$.

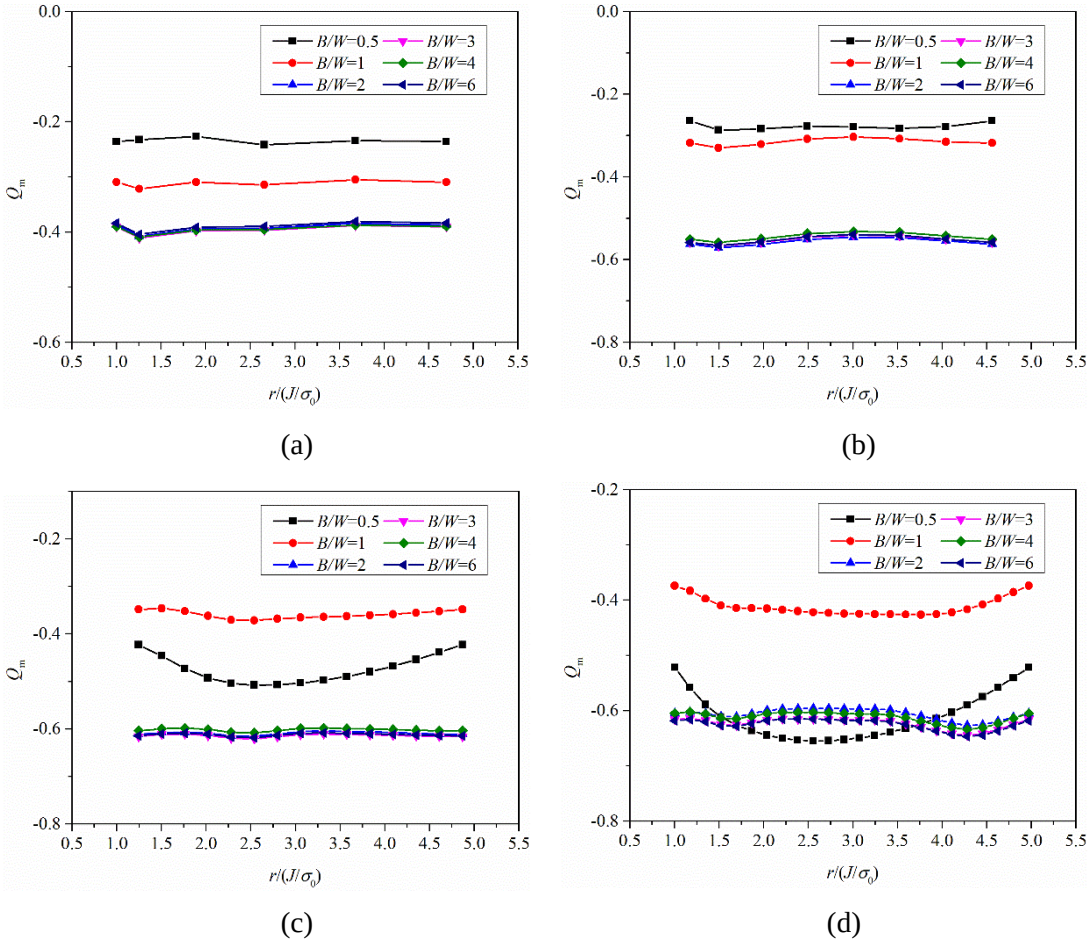

Fig. 12. Distribution of Q_m along the un-cracked ligament from the crack tip for SE(T) specimens with a/W = 0.4 and various B/W ratios at applied loading level of (a) J=50 N/mm, (b) J=200 N/mm, (c) J=400 N/mm, and (d) J=600 N/mm.

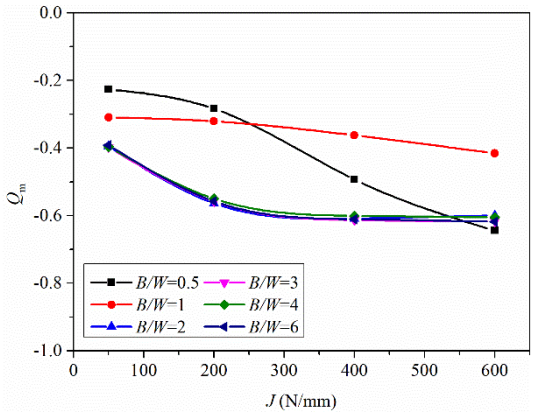

Fig. 13. Variation of Q_m with J for SE(T) specimens with a/W = 0.4 and various B/W ratios at the normalized distance of $r = 2J/\sigma_0$.

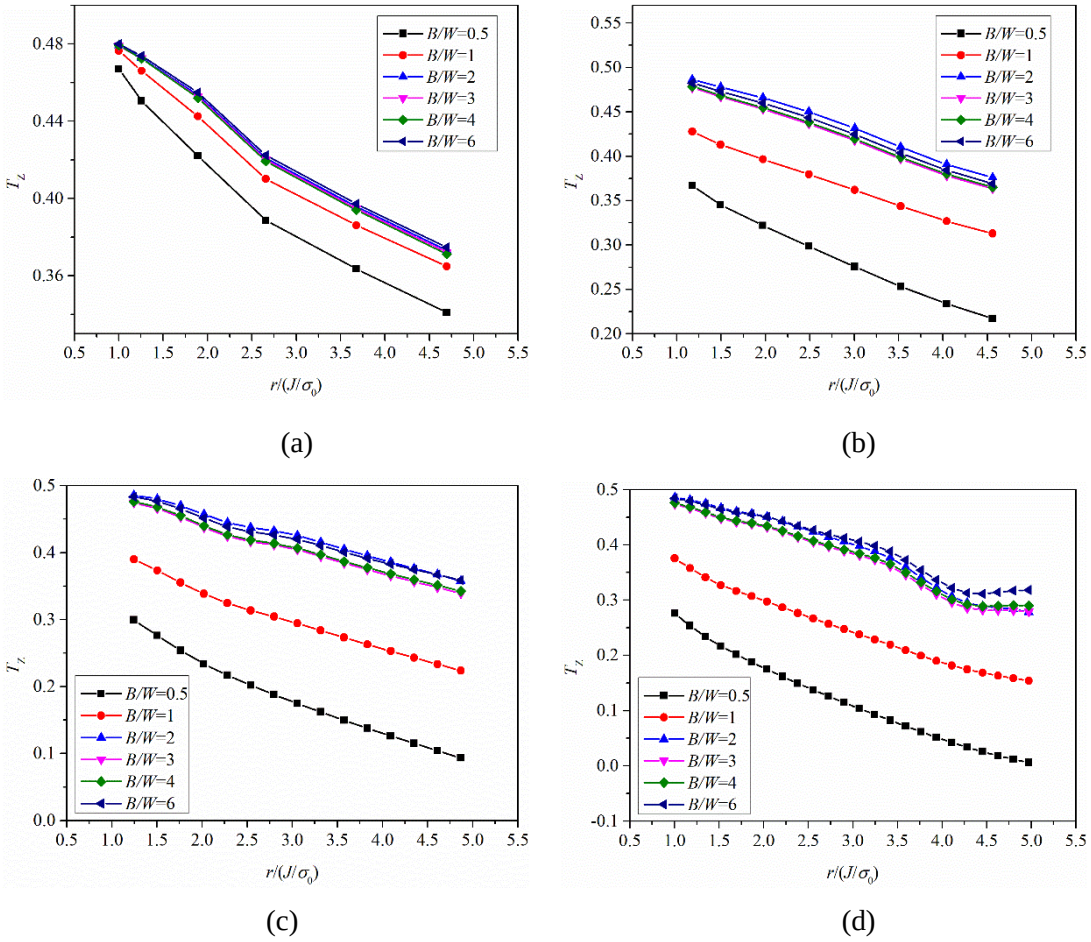

Fig. 14. Distribution of T_Z along the un-cracked ligament from the crack tip for SE(T) specimens with a/W = 0.4 and various B/W ratios at applied loading level of (a) J = 50 N/mm, (b) J = 200 N/mm, (c) J = 400 N/mm, and (d) J = 600 N/mm.

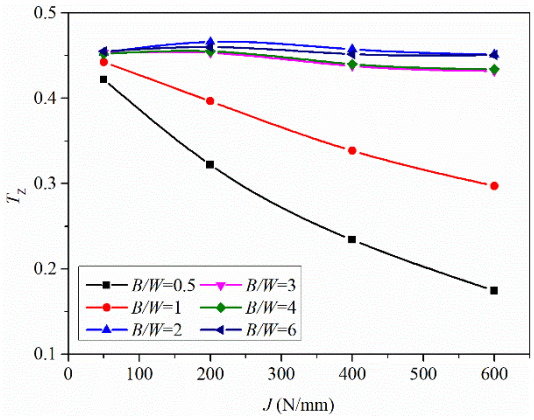

Fig. 15. Variation of T_Z with J for SE(T) specimens with a/W=0.4 and various B/W ratios at the normalized distance of r=2J/σ_0.

3.4 Results and discussion on Q_Z

3.4.1 Distance-independence

Fig. 16 shows distribution of Q_Z along the ligament. The results are determined by analyzing FEA results using the three-dimensional extension of bending modified *J-Q* solution according to Eq. (16). Four loading levels from SSY to LSY and four crack depths of the SE(T) specimens are considered. Fig. 16 indicates that the bending modified parameter Q_Z is almost distance-independent within the region of interest for specimen with the same *a/W* ratio. Fig. 17 shows the distribution of Q_Z along the ligament of the SE(T) specimens where six different thickness to width ratios (*B/W* = 0.5, 1, 2, 3, 4 and 6) are considered. It can be found in Fig. 17 that the parameter Q_Z is distance-independent for specimen with the same *B/W* ratio. Therefore, Q_Z retains the distance-independence of Q_m in contrast to Q and T_Z.

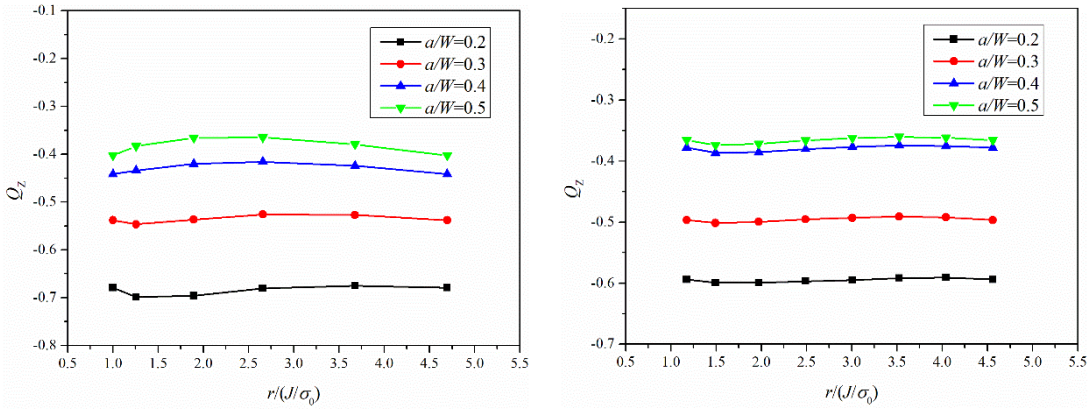

(a)

(b)

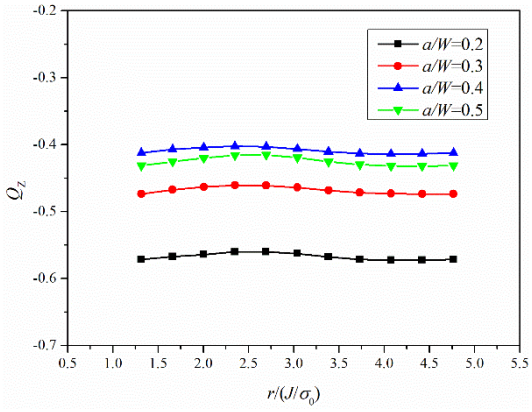

(c)

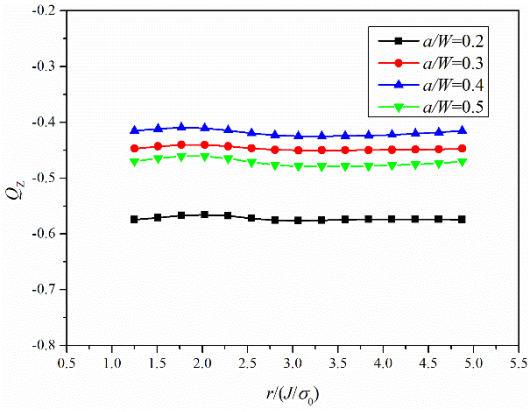

(d)

Fig. 16. Distribution of Q_Z along the un-cracked ligament from the crack tip for SE(T) specimens with B/W = 1 and various a/W ratios at applied loading level of (a) J = 50 N/mm, (b) J = 200 N/mm, (c) J = 300 N/mm, and (d) J = 400 N/mm.

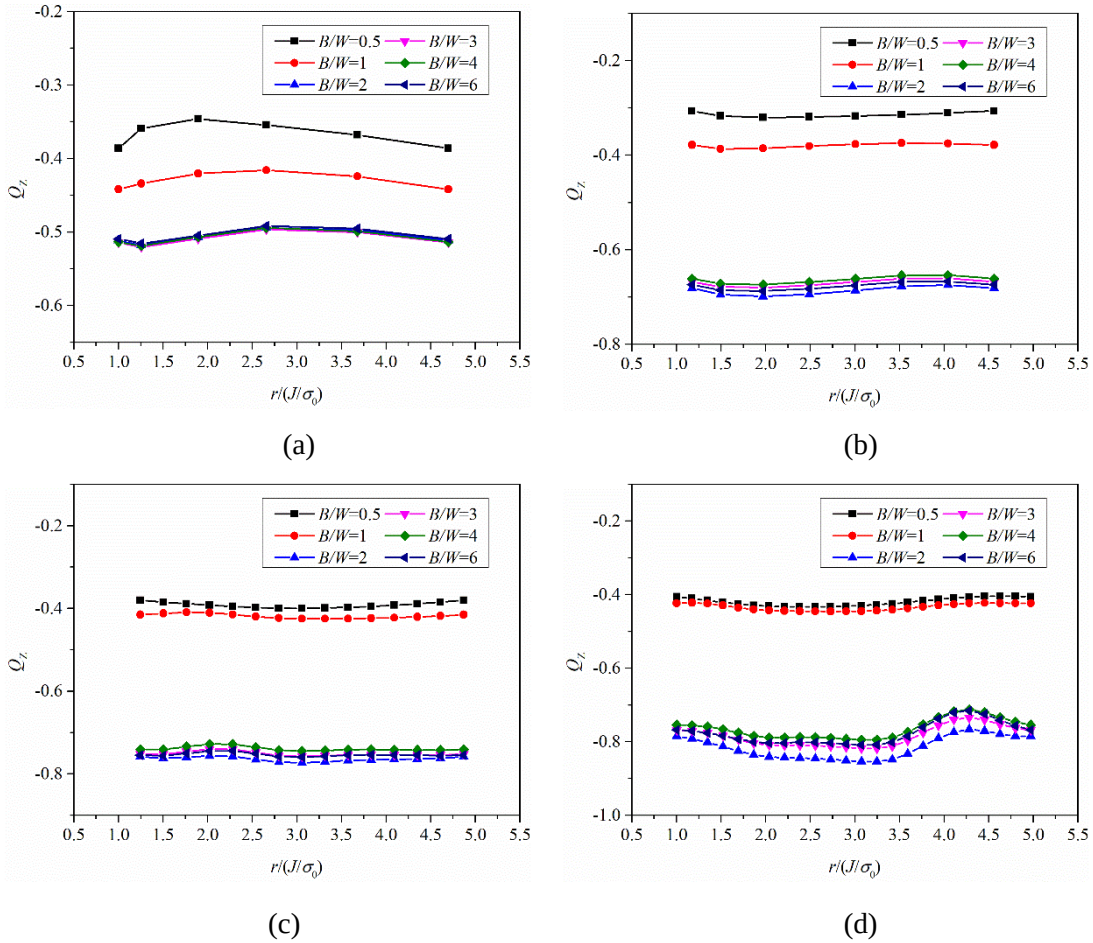

Fig. 17. Distribution of Q_Z along the un-cracked ligament from the crack tip for SE(T) specimens with a/W = 0.4 and various B/W ratios at applied loading level of (a) J = 50 N/mm, (b) J = 200 N/mm, (c) J = 400 N/mm, and (d) J = 600 N/mm.

3.4.2 Load-independence

The relationship between Q_Z vs. J of SE(T) specimens at different crack depths are presented in Fig. 18. The constraint parameter Q_Z is almost constant within the region of interest for specimen with the same a/W ratio. Fig. 19 shows the variation of Q_Z with respect to different J for specimens with different B/W.

Compared with Figs. 13 and 15, it can be found that Q_Z does not change much with the load level and can be considered as a load-independent parameter approximately.

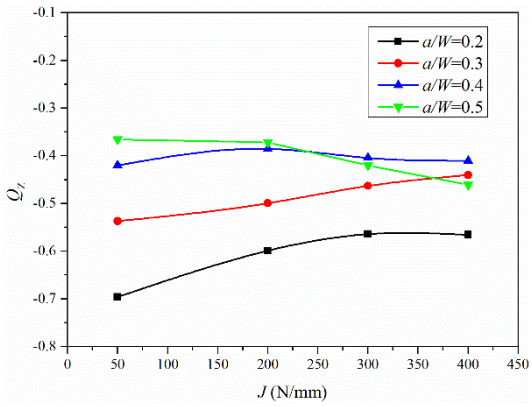

Fig. 18. Variation of Q_Z with J for SE(T) specimens with B/W = 1 and various a/W ratios at the normalized distance of $r = 2J/\sigma_0$.

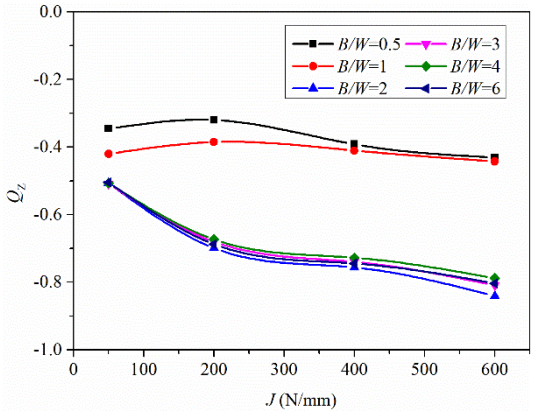

Fig. 19. Variation of Q_Z with J for SE(T) specimens with a/W = 0.4 and various B/W ratios at the normalized distance of $r = 2J/\sigma_0$.

3.4.3 Geometry-dependence

Fig. 20 plots the evolution of Q_Z with different a/W ratios (from 0.2, 0.3, 0.4 to 0.5) corresponding to different loading conditions. The specimens mentioned have the same B/W ratio of 1. The values of Q_Z increase with the increase of a/W at J = 50 and 200 N/mm. The result shows that the longer the crack length is, the larger the loss of the out-of-plane constraint level is under SSY. Fig. 21 further shows the variation of

Q_Z with B/W = 0.5, 1, 2, 3, 4, 6 under different loads for a given a/W ratio of 0.4. For B/W = 0.5 and 1, the values of Q_Z decrease slightly with the increase of the B/W ratio of SE(T) specimens. As the ratio increases to 2, the parameter Q_Z almost remains constant. The result shows that with the increase of the specimen thickness, the out-of-plane constraint level first becomes higher and after the thickness ratio reaches to 2, the out-of-plane constraint level will remain constant.

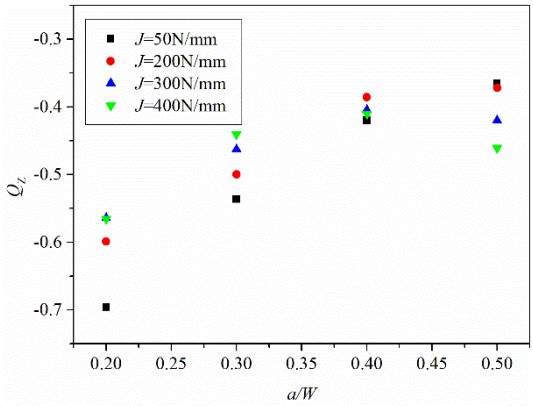

Fig. 20. Variation of Q_Z with a/W of SE(T) specimens with B/W=1 under different load at the normalized distance of $r = 2J/\sigma_0$.

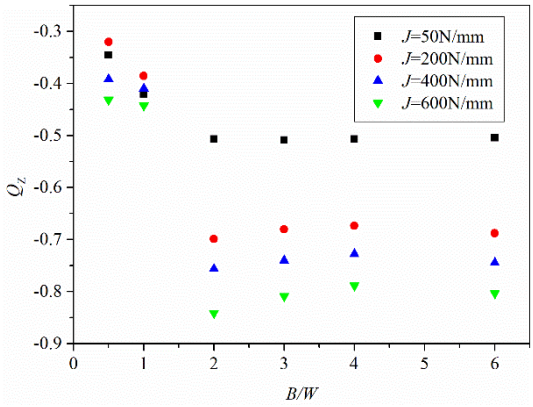

Fig. 21. Variation of Q_Z with B/W of SE(T) specimens with a/W=0.4 under different load at the normalized distance of $r = 2J/\sigma_0$.

3.4.3 The coupling effects of in-plane and out-of-plane constraints

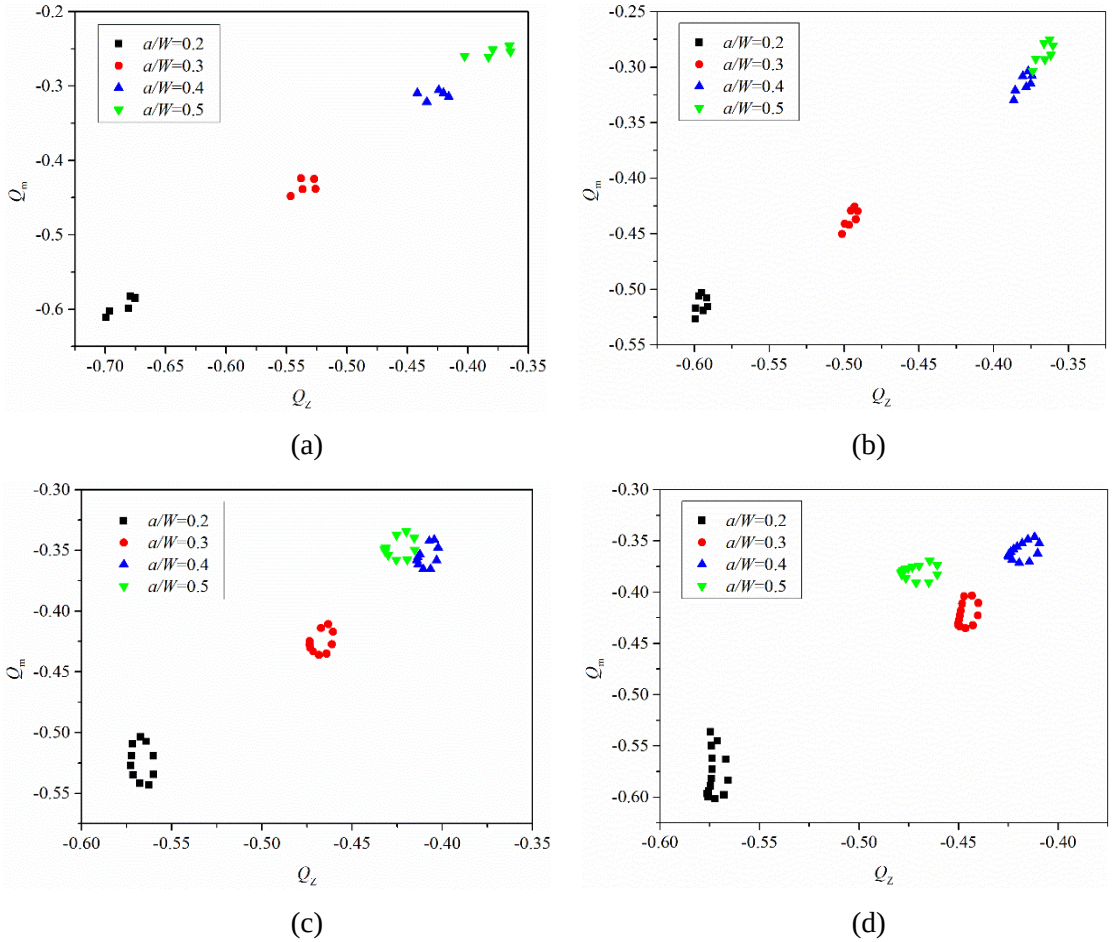

Fig. 22. Relationship between the parameters Q_m and Q_Z for specimens with B/W = 1 and various a/W ratios at applied loading level of (a) J = 50N/mm, (b) J = 200N/mm, (c) J = 300N/mm, and (d) J = 400N/mm.

The relationship between Q_m and Q_Z along the ligament of SE(T) specimens under four load levels is shown in Figs. 22 and 23. Moreover, Figs. 22(a) and (b) indicate that Q_m has a linear relationship with Q_Z where the level of in-plane constraint increases as the level of out-of-plane constraint reduces under different a/W ratios. Figs. 22(c) and (d) show that the values of the two parameters Q_m and Q_Z increase for $a/W \leq 0.4$, and decrease for $a/W \geq 0.4$ as crack depth increases under higher loads (J = 300 and 400 N/mm), which is attributed to the dominated plastic deformation in the ligament. Figs. 23(a) and (b) also show that there is a linear relationship between Q_m and Q_Z under SSY for specimens with different B/W ratios. As the thickness of the specimen increases, the level of in-plane constraint reduces, whereas the level of out-of-plane

constraint increases under SSY. As the thickness ratio increases to 2, the level of in-plane and out-of-plane constraint almost remains constant. Furthermore, it is found in Fig. 23 that as the massive plastic deformation increases, the coupling effects between Q_m and Q_Z becomes nonlinear, whereas out-of-plane constraint is in good consistency with the experiment [4].

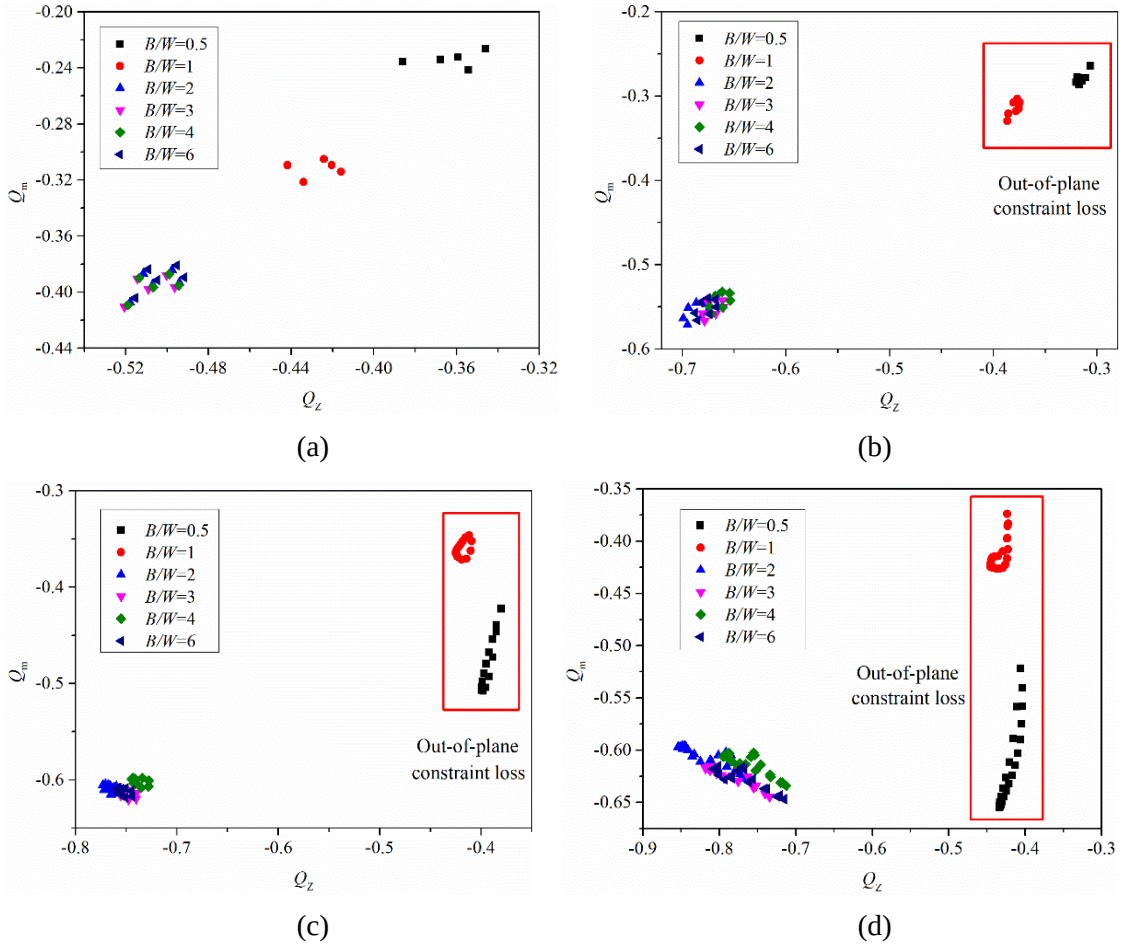

Fig. 23. Relationship between the parameters Q_m and Q_Z for SE(T) specimens with a/W=0.4 and various B/W ratios at applied loading level of (a) J=50 N/mm, (b) J=200 N/mm, (c) J=400 N/mm, and (d) J=600 N/mm.

Figs. 24 and 25 show the relationship between the parameters T_Z and Q_Z along the ligaments of SE(T) specimens under different load levels. It can be known that Q_Z is almost constant with the variation of the parameter T_Z at different normalized distance. The parameter Q_Z only changes with the length of the crack

length and the thickness of specimens under a certain load. However, T_Z is a maximum at the crack tip and then decrease along the crack growth direction, which shows significant path dependence (also can be known from Fig. 14). Therefore, Q_Z can characterize not only the out-of-plane constraint but also the bending stress. More importantly, Q_Z is a distance- and load-independent parameter and only relates to the geometry size of the specimen.

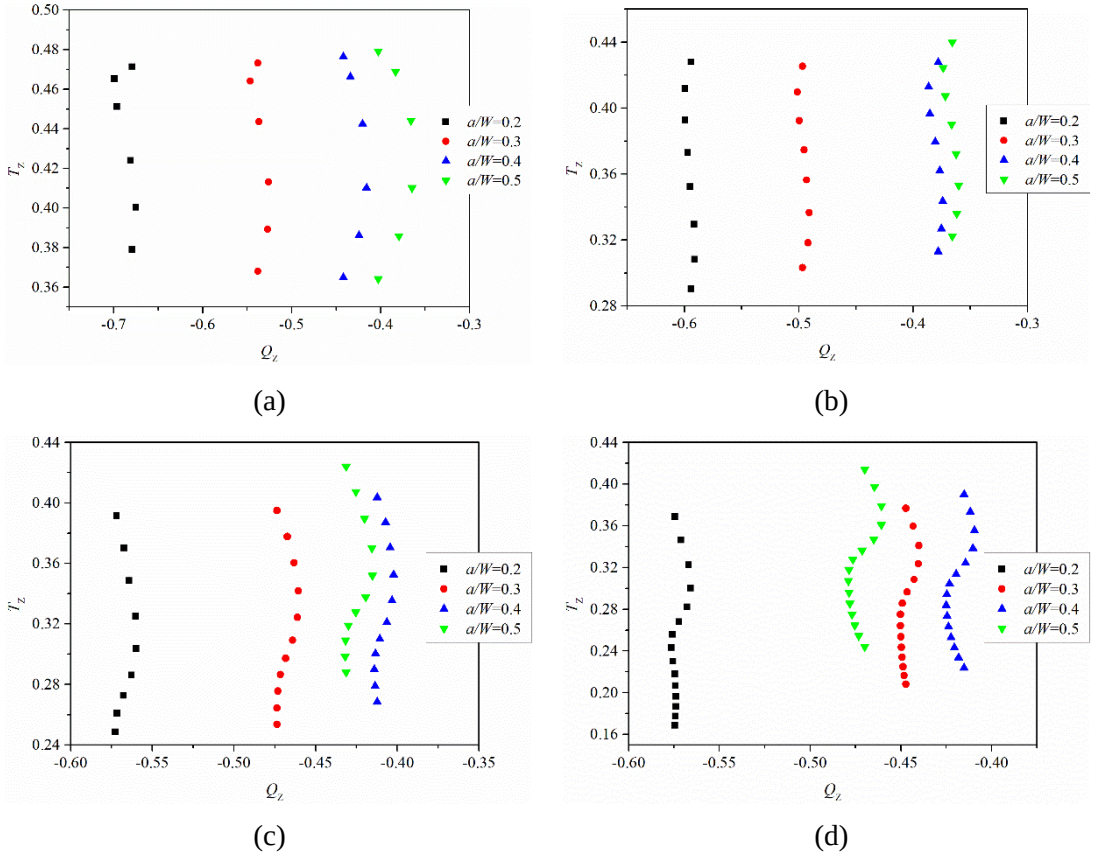

Fig. 24. Relationship between the parameters T_Z and Q_Z for specimens with B/W = 1 and various a/W ratios at applied loading level of (a) J = 50 N/mm, (b) J = 200 N/mm, (c) J = 300 N/mm, and (d) J = 400 N/mm.

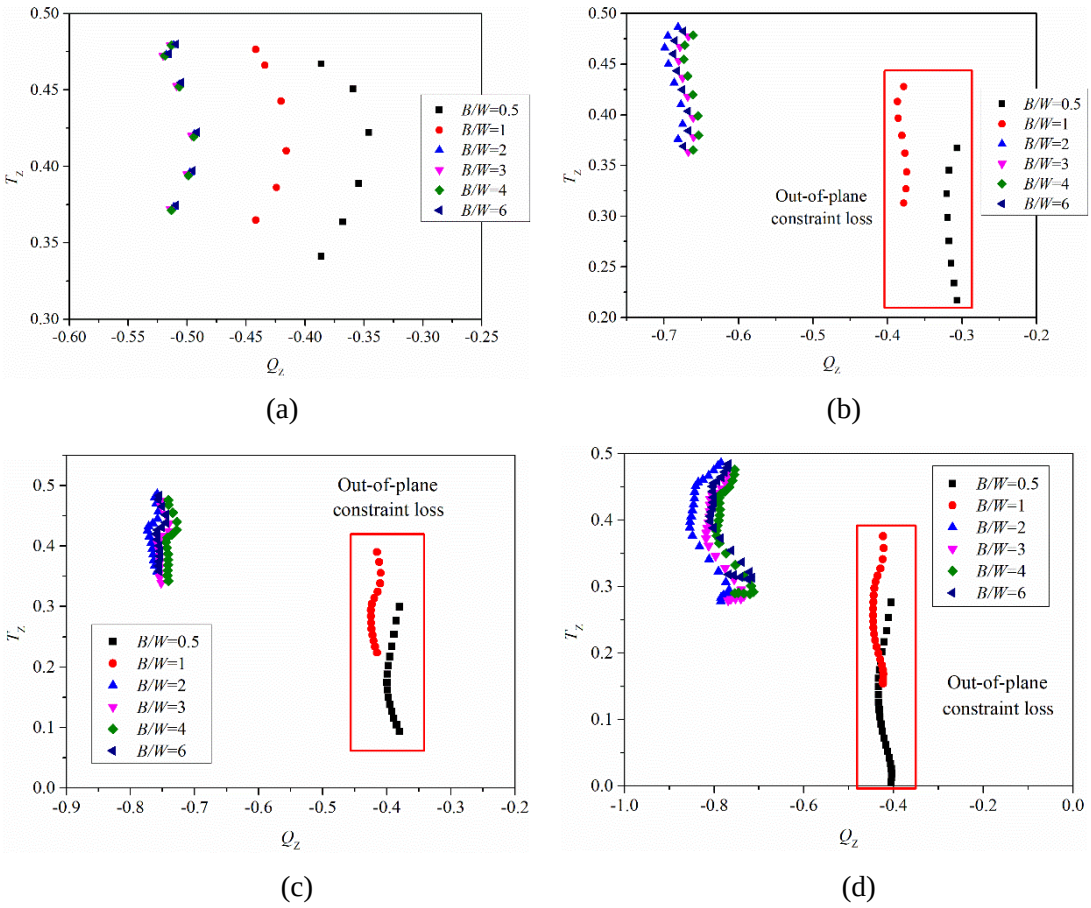

Fig. 25. Relationship between the parameters T_Z and Q_Z for specimens with a/W = 0.4 and various B/W ratios at applied loading level of (a) J=50 N/mm, (b) J=200 N/mm, (c) J=400 N/mm, and (d) J=600 N/mm.

4. Conclusions

An improved J-Q_Z-M constraint theory based on the bending modified J-Q theory and the out-of-plane constraint parameter T_Z is proposed for the clamped SE(T) specimens in the paper. The distributions of different constraint parameters Q_Z, Q, Q_m and T_Z along the ligament of the specimens obtained by the three-dimensional finite element analyses are comparatively analyzed. It is found that for SE(T) specimens with different crack lengths and different thicknesses, the parameters Q_m and Q_Z are almost distance-independent and load-independent compared to the parameters Q and T_Z. Moreover, the parameter Q_Z has better distance-independence than Q_m for specimens with smaller thickness under LSY. In addition, the parameter Q_Z is geometry-dependent. The thicker the sample is, the higher the out-of-plane

constraint level characterized by the parameter Q_Z is. After *B/W* increases to 2, the out-of-plane constraint level remains constant with further increase of the thickness, which clearly demonstrates the constraint loss of *B/W*<2.

At final, it is concluded that by virtual of the bending modified *J-Q* theory and the out-of-plane constraint parameter T_Z, the proposed three-dimensional extension of bending modified *J-Q* theory can characterize the out-of-plane constraint of SE(T) specimens with very good distance-independence, load-independence and out-of-plane constraint sensitivity. Furthermore, to validate the proposed theory, more systemic experimental tests are still deserved with variety out-of-plane and the in-plane constraints in the future.

Acknowledgements

The research is financially supported by National Key R&D Program of China (Grant No. 2018YFC0310306) and National Natural Science Foundation of China (Grant No. 52075366).

References

[1] ASTM E1820-17, Standard test method for measurement of fracture toughness, American Society for Testing and Materials, 2017.

[2] Z. Liu, X. Wang, J. Tang, C. Deng, H. Zhao, X. Chen, The effects of in-plane and out-of-plane constraints on J-R curves for X80 steel: A study using clamped SENT specimens, Eng. Fract. Mech. 206 (2019) 342–358.

[3] X. Huang, Y. Liu, X. Huang, New constraint parameters based on crack tip plastic zone: Theoretical derivations and effectiveness verification, Int. J. Solids Struct. 190 (2020) 129–147.

[4] Y. Li, B. Gong, M. Corrado, C. Deng, D. Wang, Experimental investigation of out-of-plane constraint effect on fracture toughness of the SE(T) specimens, Int. J. Mech. Sci. 128-129 (2017) 644–651.

[5] M.Y. Mu, G.Z. Wang, F.Z. Xuan, S.T. Tu, Unified correlation of in-plane and out-of-plane constraints with cleavage fracture toughness, Theor. Appl. Fract. Mech. 80 (2015) 121–132.

[6] C. Ruggieri, R.G. Savioli, R.H. Dodds, Comments on W.S. Lei's discussion of "An engineering methodology for constraint corrections of elastic–plastic fracture toughness – Part II: Effects of specimen geometry and plastic strain on cleavage fracture predictions" by C. Ruggieri, R.G. Savioli and R.H. Dodds, Engineering Fracture Mechanics 178 (2017) 535–540.

[7] S. Cravero, C. Ruggieri, Estimation procedure of J-resistance curves for SE(T) fracture specimens using unloading compliance, Eng. Fract. Mech. 74 (2007) 2735–2757.

[8] S. Cravero, C. Ruggieri, Further developments in J evaluation procedure for growing cracks based on LLD and CMOD data, Int J Fract 148 (2007) 387–400.

[9] Y. Hioe, S. Kalyanam, G.M. Wilkowski, Comparison of calculated crack growth values using unloading compliance and dc EP during SENT testing. International Pipeline Conference. American Society of Mechanical Engineers 2016 50266: V002T06A015.

[10] DNVGL-RP-F108, Assessment of flaws in pipeline and riser girth welds, Det Norske Veritas, Norway, 2017.

[11] D.Y. Park, W.R. Tyson, J.-P. Gravel, CANMET SENT test method, updates and applications, Int. J. Pressure Vessels Piping 156 (2017) 8–16.

[12] Measurement of crack-tip opening displacement (CTOD) fracture resistance curves using single-edge notched tension (SENT) specimen, ExxonMobil Upstream Research Company, America, 2010.

[13] BS 8571, Method of test for determination of fracture toughness in metallic materials using single edge notched tension (SENT) specimens, Bristish Standards Institution, London, 2014.

[14] S. Kalyanam, G. Wilkowski, F.W. Brust, Y. Hioe, E. Punch, Role of constraint in specimen geometries when evaluation fracture resistance for a surface-flawed elbow. Pressure Vessels and Piping Conference. American Society of Mechanical Engineers 2019 58974: V06AT06A065.

[15] S. Kalyanam, P. Krishnaswamy, D.-J. Shim, Y. Hioe, S. Kawaguchi, T. Shimura, K. Numata, Constraint Effects in Slow Crack Growth Test Methods for Service Life Prediction of High Density Polyethylene Piping.

[16] N.P. O'Dowd, C.F. Shih, Family of crack-tip fields characterized by a triaxiality parameter—I. Structure of fields, J. Mech. Phys. Solids 39 (1991) 989–1015.

[17] N.P. O'Dowd, C.F. Shih, Family of crack-tip fields characterized by a triaxiality parameter—II. Fracture applications, J. Mech. Phys. Solids 40 (1992) 939–963.

[18] X.K. Zhu, B.N. Leis, Bending modified J–Q theory and crack-tip constraint quantification, Int. J. Fract. 141 (2006) 115–134.

[19] W. Guo, Elastoplastic three dimensional crack border field—I. Singular structure of the field, Eng. Fract. Mech. 46 (1993) 93–104.

[20] W. Guo, Elastoplastic three dimensional crack border field—II. Asymptotic solution for the field, Eng. Fract. Mech. 46 (1993) 105–113.

[21] G.R. Irwin, Analysis of stresses and strains near the end of a crack traversing a plate., J. Appl. Mech. (1957) 361–364.

[22] J.R. Rice, G.F. Rosengren, Plane strain deformation near a crack tip in a power-law hardening material, J. Appl. Mech. 16 (1968) 1–12.

[23] Williams M.L., On the Stress Distribution at the Base of a Stationary Crack, J. Appl. Mech. 24 (1957) 109–114.

[24] Y.J. Chao, S. Yang, M.A. Sutton, On the fracture of solids characterized by one or two parameters: Theory and practice, J. Mech. Phys. Solids 42 (1994) 629–647.

[25] M.A. Verstraete, W. de Waele, R.M. Denys, K. van Minnebruggen, S. Hertelé, Constraint analysis of defects in strength mismatched girth welds of (pressurized) pipe and Curved Wide Plate tensile test specimens, Eng. Fract. Mech. 131 (2014) 128–141.

[26] X.K. Zhu, S.K. Jang, Y.F. Chen, A modification of J-Q theory and its applications, Int. J. Fract. 111 (2001) 47–52.

[27] ASTM A370, Standard test methods and definitions for mechanical testing of steel products, American Society for Testing and Materials, 1997.